RSC Advances

Development of a compact label-free small molecule measurement system using a periodically nanostructured sensor substrate

Journal:	*RSC Advances*
Manuscript ID:	RA-ART-10-2014-013449.R1
Article Type:	Paper
Date Submitted by the Author:	18-Dec-2014
Complete List of Authors:	Yokoyama, Keisuke; NSK Ltd., Oishi, Masamichi; The University of Tokyo, Institute of Industrial Science Oshima, Marie; The University of Tokyo, Institute of Industrial Science

Table of contents entry

Development of a compact label-free small molecule measurement system using a periodically nanostructured sensor substrate

K. Yokoyama, M. Oishi and M. Oshima

"Compact label-free small molecule measurement system with visible light"

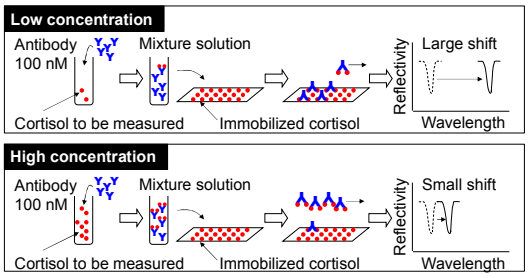

Development of a compact label-free small molecule measurement system using a periodically nanostructured sensor substrate

K. Yokoyama, M. Oishi and M. Oshima

Abstract

In order to stay in good health, people have regular checkups. Part of this process involves examining the body for abnormalities. This requires a variety of large, complicated medical equipment to measure a small amount of biomolecules or chemical substances.

The rapid advances in microelectromechanical systems (MEMS) and nanotechnology has made it possible to downsize medical equipment and perform health checkups using simpler detection methods such as label-free measurement. Nanomaterials have been used to achieve these goals; however, these require high-level sensor fabrication techniques and may provide lower sensitivity than conventional methods.

In this work, we developed a compact label-free small molecule measurement system using a periodically nanostructured sensor substrate. We fabricated the sensor substrate using simple techniques, namely, thermal nanoimprinting and sputtering. The sensor substrate realizes label-free measurement by utilizing surface plasmon resonance (SPR). A collimator is mounted into an optical fiber to reduce noise in real-time measurements. The flow cell height and velocity were investigated with the aim of shortening the equilibrium binding time. We demonstrate the simple yet effective method by performing label-free measurement of a small molecule, namely, cortisol (M.W.=362 g/mol), with a concentration of several tens of nanomolar.

We demonstrated that the normalized peak wavelength obtained by our measurement system shows good correlation with the cortisol concentration (0 nM, 24.3 nM and 48.6 nM). Our results had a smaller standard deviation than those of the ELISA test.

Introduction

Health checkups can be very time-consuming when complicated analysis methods are involved. Radioimmunoassay (RIA)[1] and enzyme-linked immunosorbent assay (ELISA)[2,3] are used to detect disease-related biomolecules or biomarkers. Both methods require additional additives such as labeled molecules and chromogenic substances in addition to antibodies (Abs). Molecule labeling is achieved either radioactively,

fluorescently, chemically or through the use of enzymes.

In order to reduce the complexity of these processes, a simple detection method, known as label-free measurement, has been developed. Label-free measurement produces a signal by directly detecting a target molecule without the use of any additional additives. Label-free measurement can be performed by liquid chromatography–mass spectrometry[4], time-of-flight mass spectrometry[5], SPR[6] and quartz crystal microbalances[7]. However, these methods require bulky bench-top equipment and have high associated costs.

As MEMS and nanotechnology have advanced, many researchers have tried to create a simple label-free detection method by utilizing nanomaterials. Carbon nanotubes[8,9], graphene[10,11], and a variety of nanowires[12-15] have been studied for use as future label-free measurement sensor materials. These materials are applicable to setups with electrical output signals; however, methods of using these are still in the research phase because of their complexity and costly fabrication.

As sensor materials that produce an optical output signal, nanoparticles[16,17] and nanostructures[18,19] have been used. With these materials, SPR can be realized simply by illuminating the sensor substrate and monitoring the change in peak wavelength. The conventional SPR experimental setup created by Kretschmann[20] and Otto[21] in 1968 is very complex; a prism is placed on the sensor substrate, which is illuminated by a light at the critical angle of total internal reflection. A moveable detector is used to monitor the change in the angle of reflection that occurs due to the reaction on the sensor substrate. For nanomaterials, uniform fabrication of the sensor platform is of the utmost importance. For nanoparticles, it is difficult to achieve uniform fabrication, meaning the output signals may be unstable due to the size distribution[16,17,22].

Since Ebessen et al.[23] discovered extraordinary optical transmission through sub-wavelength hole arrays, substrates with uniform periodic nanostructures have been studied. Electron-beam lithography[24], focused-ion-beam lithography[25], and nanosphere lithography[26] have become widely used methods for achieving uniform periodic nanostructures. However, the sensitivity of the conventional Kretschmann and Otto SPR experimental setup is higher than that of uniform periodic nanostructures. In order to enhance the sensitivity, quantum dots[27], an additional silica layer[28], and template transfer fabrication[29] have been employed. Furthermore, a combination of SPR and dielectrophoresis[30] and a combination of template-stripping fabrication, shaping the hole and different substrate materials[31] have been investigated. These methods require additional processes for the measurement and the cost increases as a result.

There are a variety of disease-related molecules in the human body. Cortisol is a small molecule with a molecular weight of 362 g/mol. Cortisol has been studied by many researchers as a biomarker of stress-related diseases, particularly for its correlation with depression. Since its concentration in saliva is several tens of nanomoles per liter[32,33], it is challenging to achieve label-free measurement using a compact measurement system with a simply-fabricated sensor substrate.

In this paper, we describe a compact and effective measurement system with a periodically nanostructured sensor substrate for performing label-free measurement of cortisol. The sensor substrate is uniformly and simply fabricated through thermal nanoimprinting and sputtering techniques. A collimator is embedded into an optical fiber to enhance the signal-to-noise ratio. The height of the flow cell and the flow velocity are examined with the aim of reducing the equilibrium binding time. We also developed a simple yet efficient method for measuring the concentration of cortisol to several tens of nanomolar. We compare our results to those obtained using the ELISA test to demonstrate the applicability of both the present system and the measurement method.

Measurement method

When molecules with a higher refractive index than the surrounding medium become attached to the sensor substrate, the peak wavelength will lengthen. When an incident light illuminates a periodically nanostructured sensor substrate with the unit structure aligned in a triangular lattice, the reflected light spectrum exhibits an SPR peak wavelength λ_{peak} given by

$$\lambda_{\mathrm{peak}} = \frac{\sqrt{3}\,d}{2\left(i^2 + j^2 - ij\right)^{1/2}} \left[\frac{\varepsilon_{\mathrm{m}}\, n^2}{\varepsilon_{\mathrm{m}} + n^2}\right]^{1/2}, \qquad (1)$$

where d is the periodicity of the unit structure, i and j are the diffraction orders, ε_{m} is the dielectric constant of the surface metal, and n is the refractive index of the surrounding medium[19]. Equation (1) shows the dependence of the peak wavelength on the surrounding refractive index.

In order to measure small molecules easily, larger-molecule-labeled antigens[34] or larger-molecule antibodies[35] are measured instead. However, the former is not a label-free measurement, and the latter requires flow control of considerable accuracy

because antigens and antibodies are transported simultaneously to the sensor substrate from two channels.

We developed a simple yet effective method to measure antibodies with larger molecular weights that are attached to the small molecules. Figure 1 is a schematic illustration of the present method. First, a known quantity of antibody (150 kDa) is added to the initial cortisol solution. Most of the cortisol in the mixture solution reacts with the added antibody. Then the mixture solution of the cortisol and antibody is transported to the sensor substrate which is pre-coated with cortisol. The immobilized cortisol on the sensor substrate binds to the antibodies in the mixture solution that still have free binding sites.

The peak wavelength shifts depending on the amount of antibody that reacts with the immobilized cortisol on the sensor substrate. In the case of a low cortisol concentration as shown in Fig. 1(a), only a small number of antibodies in the mixture solution react with the initial cortisol, meaning many antibody binding sites are still available. The result is a large peak wavelength shift. In the case of a high cortisol concentration as shown in Fig. 1(b), a small peak wavelength shift will occur. Many binding sites of the antibodies in the mixture solution are occupied by the initial cortisol molecules. Thus, a smaller number of the antibodies in the mixture solution react with the immobilized cortisol, resulting in the relatively small wavelength shift.

Measurement system

An overview of our measurement system is shown in Fig. 2(a). The sensor substrate is set inside the flow cell. The sample solution is transported to the sensor substrate using a peristaltic pump. A tungsten halogen lamp (LS-1, Ocean Optics Inc., FL, USA) is used to illuminate the substrate through a bifurcated optical fiber (WBIF200-UV-VIS, Ocean Optics Inc., FL, USA). A collimator (SMA 780NM, NA=0.55, Edmund Optics Inc., NJ, USA) is mounted in the optical fiber to produce a collimated light beam. The collimated light vertically illuminates the sensor substrate and the reflected light is collected by a spectrometer (USB4000-UV-VIS, Ocean Optics Inc., FL, USA) capable of measuring wavelengths from 400 to 900 nm.

The flow cell is shown in Fig. 2(b). The sensor substrate is placed on a polytetrafluoroethylene platform with two ports for inlet and outlet tubes. A polydimethylsiloxane (PDMS) film with a rectangular cutout and a slide glass are placed on the PDMS film, forming a flow channel that is 4 mm wide, 40 mm long. Flow channels with thicknesses of 500 μm and 2000 μm were formed to examine the effects of flow cell height on the equilibrium binding time, as discussed later in the paper. The

sensor substrate, PDMS film, and slide glass are tightly bound with two jigs. The flow cell is loaded onto the measuring equipment. The vertically mounted optical fiber illuminates the substrate with collimated incident light and receives zero-order reflected light. The reflectivity is calculated from the reflected light spectrum based on that of an aluminum reference mirror. The fabrication and design of the sensor substrate are described in the following sections.

Fabrication and design of the sensor substrate

Sensor fabrication

A sensor substrate with periodic nanostructures was prepared using thermal nanoimprint and sputtering techniques. The thermal nanoimprint technique provides a method of uniformly and simply transferring the nanostructure pattern of a mold to a thermoplastic film[36]. A mold made of silicon with silicon oxides was fabricated using electron beam lithography. In order to coat a release layer on the mold, the mold was first immersed in a release agent for 1 min and then dried for 24 h at room temperature. The mold was immersed in a rinse agent to remove excess release agent.

Figure 3(a) shows a schematic illustration of the sensor substrate fabrication. The mold was placed on a 20-mm^2 silicon substrate. Next, a piece of cyclic olefin polymer (COP) film followed by another 20-mm^2 silicon substrate were placed on the mold. They were sandwiched with 8-inch silicon wafers and carefully loaded onto the thermal nanoimprinting machine (X-300, SCIVAX corporation, Tokyo, Japan). 12 MPa of pressure was imposed on the sensor substrate at 150°C for 1 min. Subsequently, it was cooled down to 60°C, and the COP film with the transferred periodic nanostructures was removed from the mold.

The COP film was then loaded into a sputtering machine (SVC-700RF III, Sanyu Electron Co. Ltd., Tokyo, Japan) and a gold film was deposited under a pure argon atmosphere.

Sensor design

The shape of the sensor substrate was determined by atomic force microscopy (AFM, Agilent 5500, Agilent Technologies Inc., CA, USA). As shown in Fig. 3(b), the sensor substrate has periodic nanostructures. The unit structure of the sensor substrate is an equilateral triangle with a hole at each corner. The unit structure is aligned in a triangular lattice on the sensor substrate. The dimensions of the holes are defined in the cross-sectional view shown in Fig. 3(c) by using two auxiliary lines along the

sidewalls and one auxiliary line along the surface. Each hole has a diameter of 129 nm and a depth of 243 nm and the periodicity of the structure is 613 nm.

In order to immobilize the cortisol molecules on the sensor substrate, 11-amino-1-undecanethiol hydrochloride (AUT) and hydrocortisone 3-(O-carboxymethyl)oxime (CO-CMO) were used. AUT has a linear hydrocarbon chain which has a thiol group at one end and an amino group at the other end. A thiol group forms a strong bond with gold[37]. AUT molecules are well aligned to form a monolayer due to their structure. CO-CMO has a carboxymethyl oxime group allowing it to be linked with AUT via an amide bond. 4-(4,6-Dimethoxy-1,3,5-triazin-2-yl)-4-methylmorpholinium chloride n-Hydrate (DMT-MM) was used as a reaction agent for amide bond creation[38].

A sensor substrate was immersed in a 1-mM AUT ethanol solution for 20 h followed by rinsing with ethanol and water to form a monolayer with outward-exposed amino groups. A methanol mixture solution of 3-mM cortisol and 6-mM DMT-MM was prepared. The sensor substrate was immersed in the mixture solution for 7 h to complete the reaction and then rinsed with water to link the monolayer with cortisol molecules via amide bonds.

The successful addition of AUT was confirmed by X-ray photoelectron spectroscopy (XPS) and ellipsometry. Figure S1 shows the result of the XPS measurement. After AUT treatment on the sensor substrate, the element N and S which are included in AUT were detected. Figure S2 shows the result of the ellipsometry measurement. The thickness of the AUT monolayer is 1.6 nm which is the same thickness as reported elsewhere[39]. The reaction of AUT and CO-CMO was characterized by time-of-flight mass spectrometry (TOFMS). In order to remove the side reaction of the thiol group of AUT, Dodecylamine which has methyl group instead of the thiol group of AUT was used. The mixture solution of Dodecylamine and CO-CMO was characterized by TOFMS. Figure S3 shows the result of the measurement indicating the coupling reaction of Dodecylamine and CO-CMO successfully completed. In the following experiments, phosphate buffered saline (PBS) was used as the solvent unless otherwise noted.

Results and discussion

Effects of the collimator

Sensitivity is generally given in terms of a signal-to-noise ratio. In real-time monitoring, the signal is the change in peak wavelength due to the molecular reaction while the noise is a change in the peak wavelength at the steady state.

In the present measuring system, the peak wavelength is calculated for the

zero-order reflected light spectrum. The stronger the intensity of the reflected light, the more stable the peak wavelength. The incident light vertically illuminates the sensor substrate through an optical fiber. The diameter of the illuminated sensing spot on the sensor substrate increases with an increase in the distance between the optical fiber and the sensor substrate. Thus, the intensity of the collected zero-order reflected light decreases with an increase in this distance, leading to a low signal-to-noise ratio.

In order to improve the signal-to-noise ratio, a collimator is mounted into the optical fiber. With a collimator-embedded optical fiber, the intensity of the collected light is less affected by the distance. Most of the reflected light from the sensor substrate can be collected using this method. Figure 4 shows the behavior of the peak wavelength measured in real-time in water for 350 s for several experimental setups. With the collimator-embedded optical fiber, the peak wavelength stayed almost constant even when the distance to the sensor substrate was 30 mm. With a conventional optical fiber (an optical fiber without a collimator), the signal exhibited a significant level of noise at just 15 mm. The standard deviation (SD) of the peak wavelength fluctuation was calculated over 350 seconds in Fig. 4. The SD was 0.0068 for the collimator-embedded optical fiber and 0.0952 for the conventional optical fiber, revealing an improvement of one-fourteenth obtained by the collimator. It is concluded that the high intensity of the reflected light collected through the collimator yields a stable real-time signal with a high signal-to-noise ratio.

Effects of flow cell height and flow velocity on the equilibrium binding time

We investigated the influence of the height of the flow cell and the flow velocity on the equilibrium binding time. Without flow, molecules in the analyte can move to the sensor substrate under Brownian motion. According to Fick's second law of diffusion, the diffusion time t is expressed as follows,

$$t = \frac{L^2}{D} \qquad (2)$$

where D is the diffusion coefficient and L is the diffusion length. The chance of reaction for molecules in the analyte increases as the diffusion length decreases, which is achieved by reducing the height of the flow cell in the present system. In order to reduce the equilibrium binding time, we used two types of flow cell which have PDMS films of different heights. One film is 500 μm in height while the other is 2000 μm. The 100-nM antibody solution in which the antibody is dissolved in 10-mM PBS is

transported to the immobilized cortisol on the sensor substrate. Figure 5(a) shows the result of the cortisol-antibody reaction. The equilibrium binding time with the 500-μm-high flow cell is approximately 6000 s. This is almost one quarter of that with the 2000-μm-high flow cell.

Next, we investigated the effects of flow velocity on the equilibrium binding time. Hu et al.[40] reported that the equilibrium binding time decreases with increasing flow velocity. We used three flow velocities, 0, 2.5 and 10 mm/s for the cortisol-antibody reaction. Figure 5(b) shows the relationship between the flow velocity and the equilibrium binding time. The equilibrium binding time at 0 mm/s is approximately 6000 s while that at 10 mm/s is approximately 1000 s. The equilibrium binding time fell to one-sixth of its initial value with an increase in the flow velocity of 10 mm/s. It is hypothesized that the equilibrium binding time decreases due to the continuous supply of unreacted molecules in the analyte to the sensor substrate.

The equilibrium binding time of 23000 s for a 2000-μm-high flow cell with no flow decreases to 1000 s when a 500-μm-high flow cell is used instead and a 10-mm/s flow velocity is introduced.

Results of immunoassay

We investigated the effects of the collimator, the flow height, and the flow velocity on the measurement as shown in Table 1. For the immunoassay demonstration, we used the collimator-embedded optical fiber, 500-μm-high flow cell and 10 mm/s flow velocity. In order to verify the accuracy of the present method, we prepared three concentrations of cortisol solution, 0, 24.3 and 48.6 nM. The same amount of antibody was added to each solution such that all solutions had an antibody concentration of 100 nM. The mixture solution was transported to the sensor substrate and the peak wavelength shift was monitored. After the immobilized cortisol on the sensor substrate reacted with the antibodies in the mixture solution, an additional pure 100-nM antibody solution was applied. This additional solution allows the peak wavelength shift to be normalized such that the individual deviation of sensor substrates was minimized.

As shown in Fig. 6, the peak wavelength lengthened due to the reaction of the antibodies in the mixture solution with the immobilized cortisol on the sensor substrate. The peak wavelength at the initial PBS treatment showed different values. It is considered that the variation in dimension of the individual nanostructure of the sensor substrate affects the initial peak wavelength. After the first reaction finished, the additional antibody solution was applied for normalization. The peak wavelength again shifted to a longer wavelength, indicating that the available binding sites of the

immobilized cortisol reacted with the added antibodies.

In Fig. 6(c), $\Delta\lambda_{peak\_1}$ is the peak wavelength shift resulting from the reaction of the antibodies in the mixture solution with the immobilized cortisol on the sensor substrate. $\Delta\lambda_{peak\_2}$ is the sum of $\Delta\lambda_{peak\_1}$ and the further shift in peak wavelength caused by the reaction of the antibodies in the additional solution with the remaining binding sites of the immobilized cortisol on the sensor substrate.

Figure 7 shows the relationship between the initial cortisol concentration and the absolute peak wavelength shift $\Delta\lambda_{peak\_1}$ as well as the normalized peak wavelength shift $\Delta\lambda_{peak\_1}/\Delta\lambda_{peak\_2}$. Both values, $\Delta\lambda_{peak\_1}$ and $\Delta\lambda_{peak\_1}/\Delta\lambda_{peak\_2}$, are highly correlated with the initial cortisol concentration. The values of the normalized peak wavelength $\Delta\lambda_{peak\_1}/\Delta\lambda_{peak\_2}$ have a far smaller standard deviation than those of the absolute peak wavelength $\Delta\lambda_{peak\_1}$. These findings confirm that the present measurement system functions effectively for small molecules even at nanomolar concentrations. Furthermore, the standard deviation can be reduced by normalizing the absolute peak wavelength values using those of an additional pure 100-nM antibody solution.

The ELISA test (Salimetrics LLC, PA, USA) was conducted to evaluate our results. Four standard cortisol solutions supplied with the ELISA kit for calibration were used. Their concentrations were 3.1, 9.2, 27.9 and 82.9 nM. The ELISA kit uses a competitive assay. In a competitive assay, the cortisol molecules in the standard cortisol solutions compete with enzyme-labeled cortisol molecules of a fixed concentration to bind to an antibody attached to the plate. The cortisol solutions were pipetted into the wells of a plate. Then, the enzyme-labeled cortisol molecules were added to the initial standard cortisol solution. The two types of cortisol competed to bind to the antibodies immobilized on the plate. Subsequently a chromogenic substance was added to produce an optical signal. The optical signals were collected and analyzed with a photometric measurement device (Multiskan Ascent, Thermo Fisher Scientific Inc., MA, USA).

In Fig. 8, our results for P_{NSK} are compared to those of the ELISA test R_{ELISA}. Our results had a smaller standard deviation than those of the ELISA test. In the present measurement system, both the sample solution and the wash buffer can be continuously

transported to the sensor substrate. The ELISA test, however, uses isolated wells, meaning each process is performed discontinuously with a pipette. Such discontinuity could lead to errors and result in a large standard deviation. Regarding the duration of the measurements, it took three to four hours for a series of cortisol-antibody reactions to take place using the present system, which is comparable to the ELISA test. Furthermore, the present measurement system is approximately one-fifth the volume and less than half the weight of the ELISA device.

Conclusions

We developed a compact label-free measurement system for small molecules that uses a periodically nanostructured sensor substrate. The fabrication of the sensor substrate is simply based on thermal nanoimprint and sputtering techniques. We embedded a collimator into an optical fiber and reduced the noise in real-time measurements by one-fourteenth as a result. Furthermore, the equilibrium binding time was reduced to one-twenty third of its original value by decreasing the height of the flow cell and introducing a flow velocity. The present measurement system is one-fifth of the volume and less than half the weight of the conventional device used for the ELISA test.

We developed a simple yet effective method for detecting small cortisol molecules at low concentrations by measuring attached larger-molecule antibodies instead of direct detection. We successfully conducted label-free measurement of cortisol at a concentration of several tens of nanomolar. Furthermore, we reduced the output signal standard deviation by adding a pure antibody solution for normalization.

We conducted the ELISA test to validate the present measurement method. The present measurement system had a smaller standard deviation than the ELISA test in terms of the output signal values. The time required for the cortisol measurement is comparable to the duration of the ELISA test. These results demonstrate that the developed measurement system is competitive in terms of compactness and performance.

Acknowledgements

We thank Prof. Fujii and Dr. Kinoshita from The University of Tokyo, as well as Mr. Furukawa, Ms. Okutani, Mr. Sasao, Dr. Oguchi, and Dr. Takajo from NSK Ltd. for advice and comments on the research. This work was supported by The University of Tokyo and NSK Ltd.

Notes and references

[a] *NSK Ltd., 1-5-50, Kugenuma Shinmei, Fujisawa-shi, Kanagawa, 251-8501, Japan. Fax: +81-466-21-3385; Tel: +81-466-21-3072; E-mail: yokoyama-ke@nsk.com*

[b] *Institute of Industrial Science, The University of Tokyo, Komaba 4-6-1, Meguro-Ku, Tokyo 153-8505, Japan. Fax: +81-3-5452-6205; Tel: +81-3-5452-6205*

† Electronic Supplementary Information (ESI) available: [details of any supplementary information available should be included here]. See DOI: 10.1039/b000000x/

‡ Footnotes should appear here. These might include comments relevant to but not central to the matter under discussion, limited experimental and spectral data, and crystallographic data.

1 A. H. B. Wu, *Clin. Chim. Acta*, 2006, **369**, 119-124.

2 A. Ambrosi, F. Airò and A. Merkoçi, *Anal. Chem.*, 2010, **82**, 1151-1156.

3 R. Rica and M. M. Stevens, *Nat. Nanotechnol.*, 2012, **7**, 821-824.

4 H. J. Issaq, O. Nativ, T. Waybright, B. Luke, T. D. Veenstra, E. J. Issaq, A. Kravstov and M. Mullerad, *J. Urol.*, 2008, **179**, 2422-2426.

5 C. F. Streckfus, L. R. Bigler and M. Zwick, *J. Oral Pathol. Med.*, 2006, **35**, 292-300.

6 M. A. Cooper, *Anal. Bioanal. Chem.*, 2003, **377**, 834-842.

7 X. Su, Y. Li, *Biosens. Bioelectron.*, 2005, **21**, 840-848.

8 M. Yang, S. Sun, H. A. Bruck, Y. Kostova and A. Rasooly, *Lab Chip*, 2010, **10**, 2534-2540.

9 M. T. Martínez, Y. Tseng, N. Ormategui, I. Loinaz, R. Eritja and J. Bokor, *Nano Lett.*, 2009, **9**, 530-536.

10 Q. Wei, K. Mao, D. Wu, Y. Dai, J. Yang, B. Du, M. Yang and H. Li, *Sensor Actuat. B-Chem.*, 2010, **149**, 314-318.

11 Y. Liu, X. Dong and P. Chen, *Chem. Soc. Rev.*, 2012, **41**, 2283-2307.

12 R. Tian, S. Regonda, J. Gao, Y. Liu and W. Hu, *Lab Chip*, 2011, **11**, 1952-1961.

13 X. Luo and J. J. Davis, *Chem. Soc. Rev.*, 2013, **42**, 5944-5962.

14 Y. Sun, *Nanoscale*, 2010, **2**, 1626-1642.

15 X. Luo, I. Lee, J. Huang, M. Yun and X. T. Cui, *Chem. Commun.*, 2011, **47**, 6368-6370

16 C. Loo, A. Lin, L. Hirsch, M. H. Lee, J. Barton, N. Halas, J. West and R. Drezek, *Technol. Cancer Res. Treat.*, 2004, **3**, 33-40.

17 J. J. Mock, D. R. Smith and S. Schultz, *Nano Lett.*, 2003, **3**, 485-491.

18 J. C. Sharpe, J. S. Mitchell, L. Lin, N. Sedoglavich and R. J. Blaikie, *Anal. Chem.*, 2008, **80**, 2244-2249.

19 K. Nakamoto, R. Kurita, O. Niwa, T. Fujii and M. Nishida, *Nanoscale*, 2011, **3**, 5067-5075.

20 H. Raether and E. Kretschmann, *Zeitschrift für Naturforsch*, 1968, **23**, 2135-2136.

21 A. Otto, *Zeitschrift für Physik*, 1968, **216**, 398-410.

22 C. J. Murphy, T. K. Sau, A. M. Gole, C. J. Orendorff, J. Gao, L. Gou, S. E. Hunyadi and T. Li, *J. Phys. Chem. B*, 2005, **109**, 13857-13870.

23 L. H. Dubois and R. G. Nuzzo, *Annu. Rev. Phys. Chem*., 1992, **43**, 437-463.

24 J. Grand, P. Adam, A. Grimault, A. Vial, M. L. Chapelle, J. Bijeon, S. Kostcheev and P. Royer, *Plasmonics*, 2006, **1**, 135-140.

25 T. Ohno, J. A. Bain and T. E. Schlesinger, *J. Appl. Phys*., 2007, **101**, 083107/1.

26 E. M. Hicks, X. Y. Zhang, S. L. Zou, O. Lyandres, K. G. Spears, G. C. Schatz and R. P. Van Duyne, *J. Phys. Chem. B*, 2005, **109**, 22351-22358.

27 L. Niu, K. Cheng, Y. Wu, T. Wang, Q. Shi, D. Liu, Z. Du, *Biosens. Bioelectron.*, 2013, **50**, 137-142.

28 V. E. Bochenkov, M. Frederiksen, D. S. Sutherland, *Opt. Express*, 2013, **21**(12), 14763.

29 P. Jia, H. Jiang, J. Sabarinathan, J. Yang, *Nanotechnology*, 2013, **24**, 195501

30 A. Barik, L. M. Otto, D. Yoo, J. Jose, T. W. Johnson, S. Oh, *Nano Lett.*, 2014, **14**, 2006−2012.

31 G. A. C. Tellez, S. Hassan, R. N. Tait, P. Berini, R. Gordon, *Lab Chip*, 2013, **13**, 2541-2546.

32 W. T. Ebbesen, J. H. Lezec, F. H. Ghaemi, T. Thio and A. P. Wolff, *Nature*,1998, **392**, 667-669.

33 Z. Bhagwagar, S. Hafizi and J. P. Cowen, *Psychopharmacology*, 2005, **182**, 54-57.

34 H. Wua, H. Li, F. Z. H. Chu, S. F. Y. Li, *Sensor Actuat B-Chem*, 2013, **178**, 541- 546.

35 R. C. Stevens, S. D. Soelberg, S. Near, C. E. Furlong, *Anal. Chem*., 2008, **80**, 6747-6751.

36 J. Egeland, A. Lund, I. N. Landro, R. B. Rund, K. Sundet, A. Asbjornsen, N. Mjellem, A. Roness and I. K. Stordal, *Acta Psychiat. Scand*., 2005, **112**, 434-441.

37 L. H. Dubois and R. G. Nuzzo, *Annu. Rev. Phys. Chem*., 1992, **43**, 437-463.

38 M. Kunishima, C. Kawachi, K. Hioki, K. Terao and S. Tani, *Tetrahedron*, 2011, **57**, 1551-1558.

39 A. Lesuffleur, H. Im, N. C. Lindquist and S. Oh, *Appl. Phys. Lett.*, 2007, **90**:243110.

40 G. Hu, Y. Gaob and D. Li, *Biosens. Bioelectron*., 2007, **22**, 1403-1409.

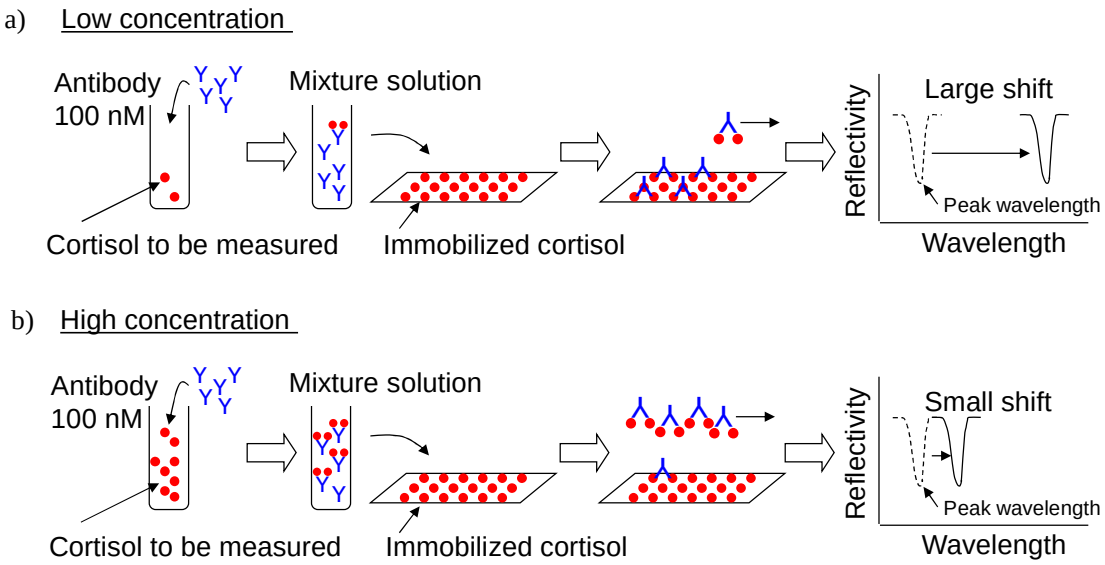

Fig. 1 Schematic illustration of the present method: Antibodies are added to the sample solution to give an antibody concentration of 100 nM, and then the mixture solution is transported to the sensor substrate which has been immobilized with cortisol beforehand. a) Low cortisol concentration: many antibody binding sites are still available in the mixture solution so it will cause a large shift in the peak wavelength. b) High concentration of cortisol: a small number of binding sites are available in the mixture solution so only a small shift in the peak wavelength will occur.

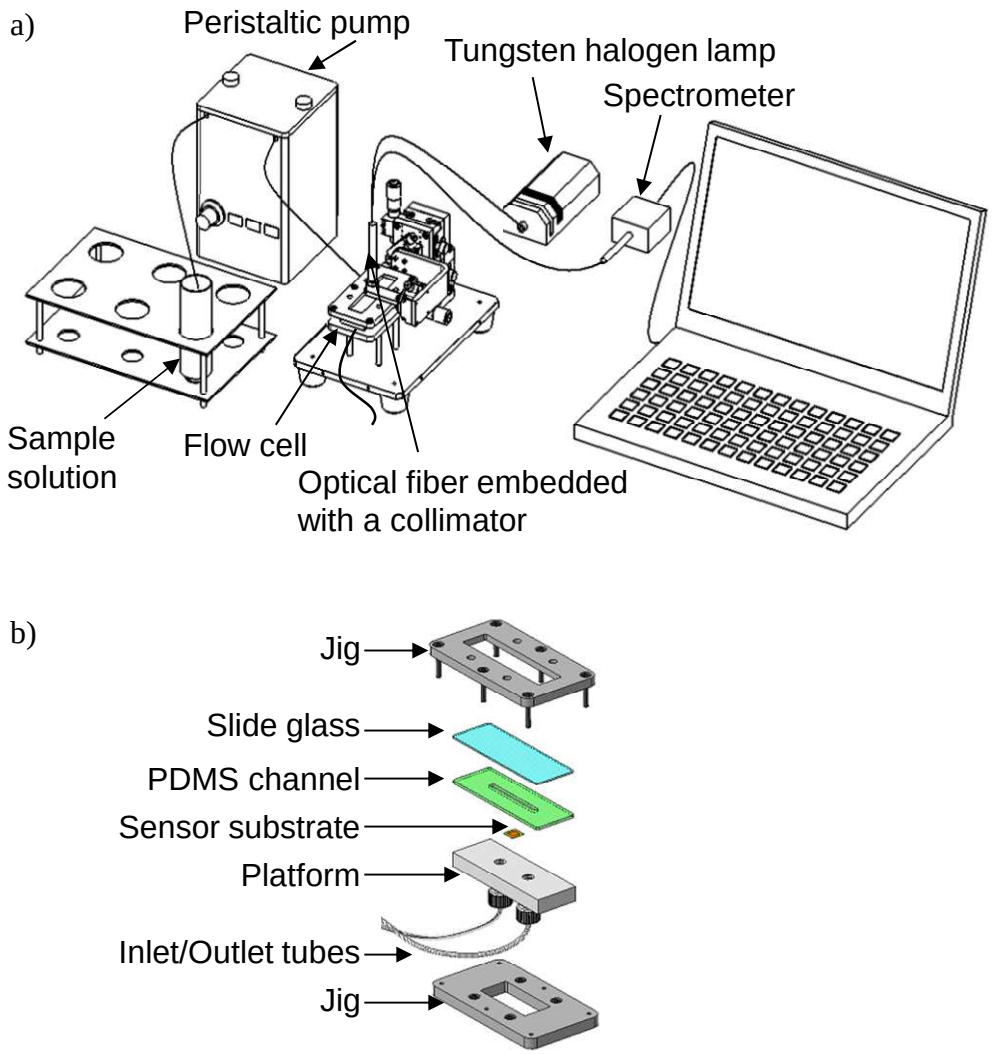

Fig. 2 Schematic illustration of the experimental setup. a) Measurement system: A tungsten halogen lamp illuminates a sensor substrate via an optical fiber. A spectrometer collects the reflected light from the sensor substrate and sends data to the PC. A sample solution is transported using a peristaltic pump. b) Flow cell: The sensor substrate is placed on a polytetrafluoroethylene platform with two ports for inlet and outlet tubes and a polydimethylsiloxane (PDMS) film with a rectangular cutout and a slide glass are layered to create a flow channel with a width of 4 mm, a length of 40 mm, and a thickness of 500 μm. Two jigs tightly bind the sensor substrate and components.

a)

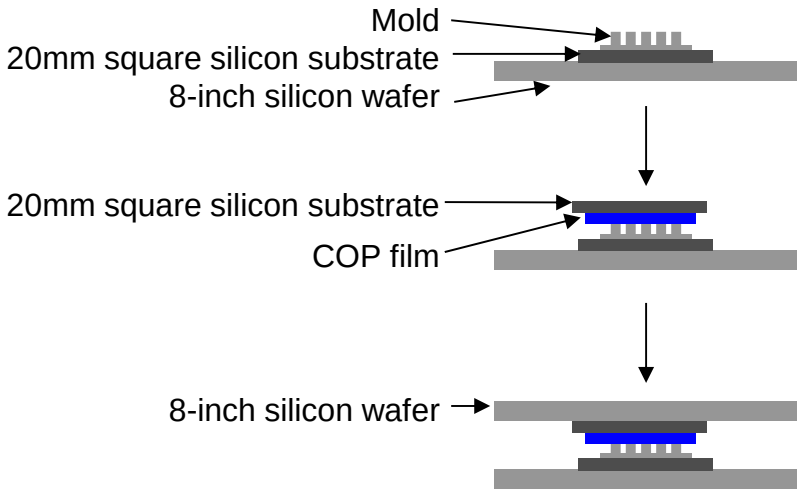
Mold
20mm square silicon substrate
8-inch silicon wafer
20mm square silicon substrate
COP film
8-inch silicon wafer

b)

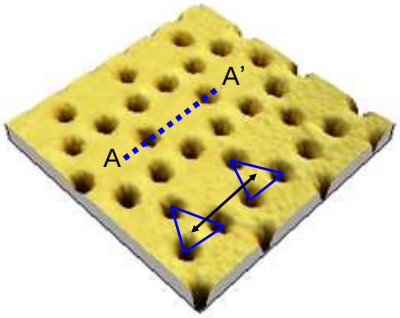
A'
A

c)

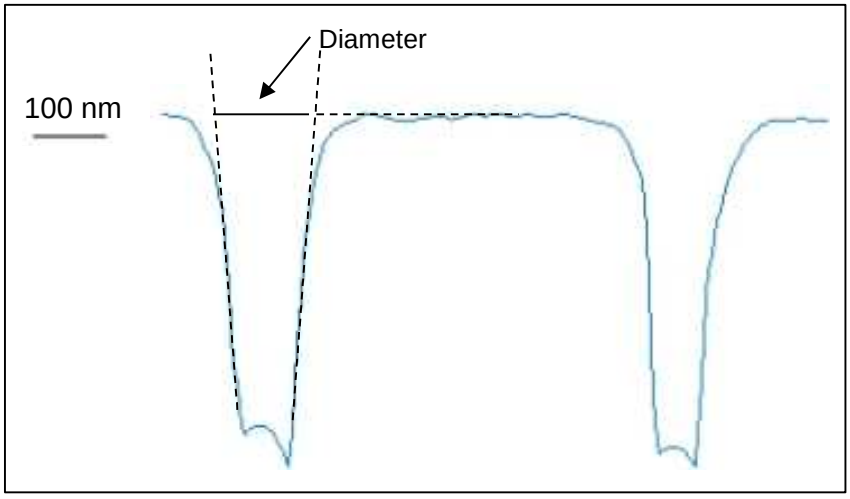
Diameter
100 nm

Fig. 3 a) Schematic illustration of the periodically nanostructured sensor fabrication procedure. The mold is placed on a 20-mm^2 silicon substrate, followed by a piece of COP film and another piece of 20-mm^2 silicon substrate. The layers are sandwiched with 8-inch silicon wafers. 12 MPa of pressure is imposed at 150°C 1 min. Subsequently, the structure is cooled to 60°C and the COP film with the transferred periodic nanostructures is removed from the mold. b) A top-down view of the AFM image of the sensor substrate which has an equilateral triangle unit structure (blue triangles) with a triangular lattice alignment. The periodicity is 613 nm (shown by the black arrowed line). Each hole is 129 nm in diameter and 243 nm in depth. c) Cross-sectional view of the blue dotted line A-A'. The dashed lines are auxiliary lines used to define the hole diameter. The scale bar is 100 nm.

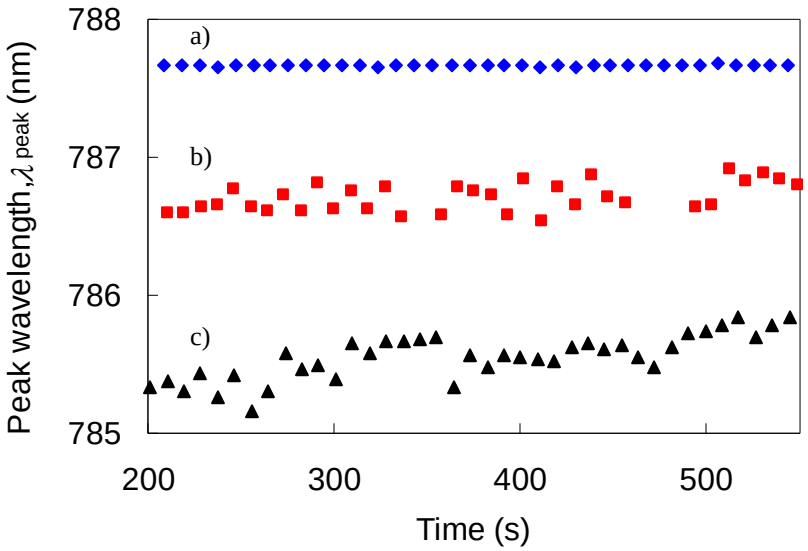

Fig. 4 Behavior of the real-time peak wavelength in water for 350 seconds. a) With a collimator (30 mm). b) Without a collimator (15 mm). c) Without a collimator (30 mm). (Values in parentheses are the distances from the optical fiber to the sensor substrate.)

a)

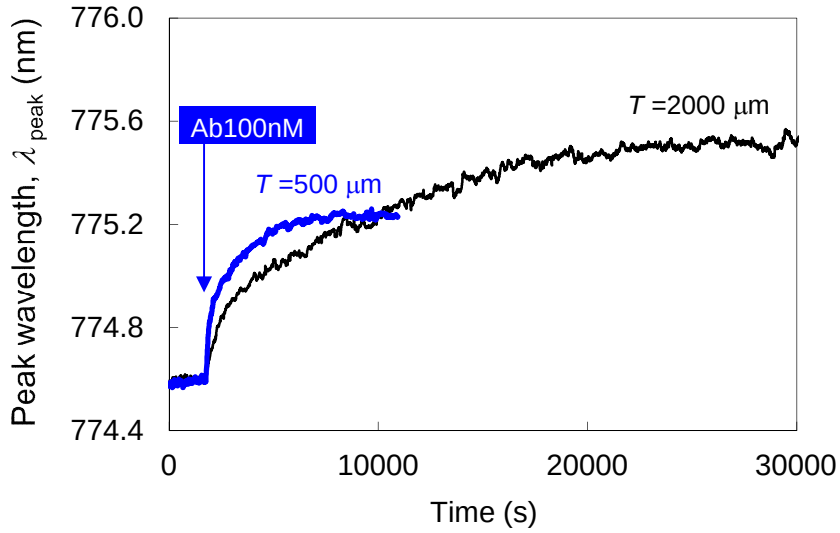

b)

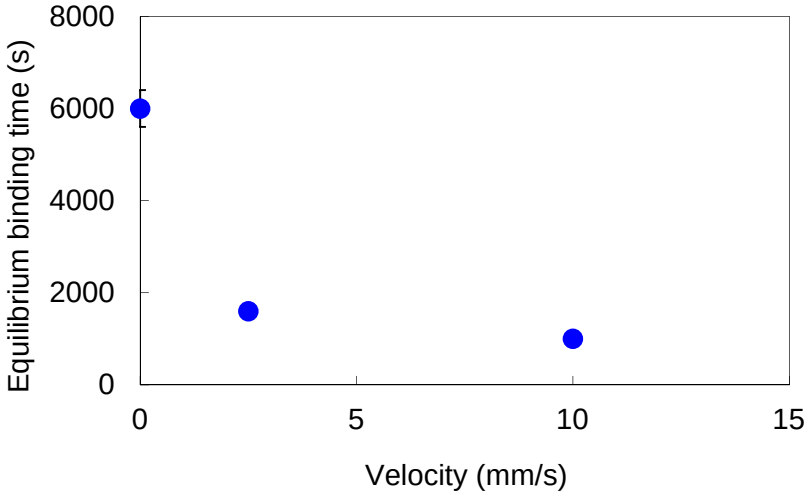

Fig. 5 a) Peak wavelength shift due to the cortisol-antibody reaction. The equilibrium binding time for a flow cell height of 500 μm is approximately 6000 s, whereas that for a 2000-μm-high cell is approximately 23000 s. The arrow indicates the injection of the antibody solution. T represents the height of the flow cell. b) Relationship between the flow velocity and the equilibrium binding time of the cortisol-antibody reaction. The equilibrium binding time at flow velocities of 0, 2.5, and 10 mm/s are approximately 6000, 1600, and 1000 s, respectively.

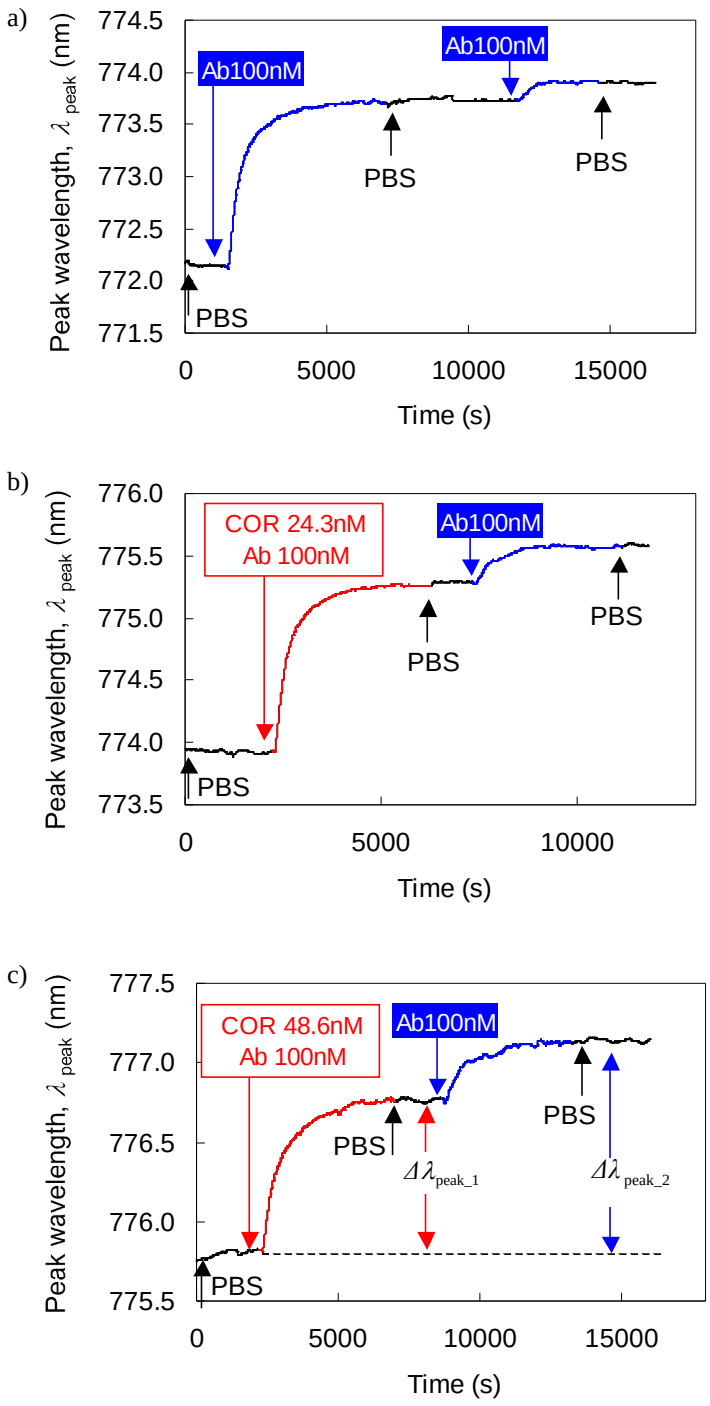

Fig. 6 Real-time peak wavelength shift with a series of solutions: PBS solution, antibody or mixture solution, PBS solution, antibody solution and PBS solution. a) 0 nM cortisol / 100 nM antibody. b) 24.3 nM cortisol / 100 nM antibody. c) 48.6 nM cortisol / 100 nM antibody.

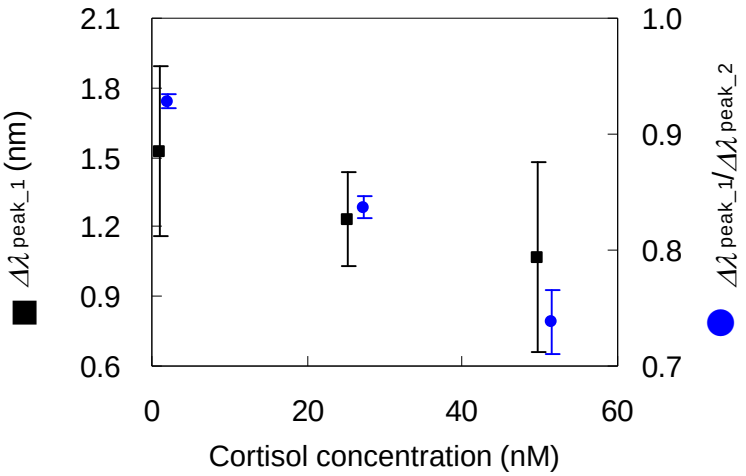

Fig. 7 Comparison between the cortisol concentration dependence of the absolute peak wavelength shift (black squares, left axis) and the normalized peak wavelength shift (blue circles, right axis). Values are translated to the right by 1 nM and 3 nM for display purposes, respectively.

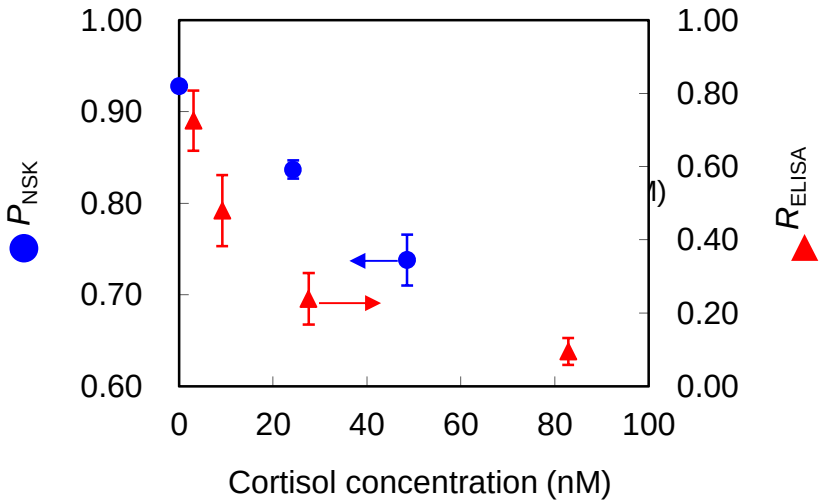

Fig. 8 Comparison of the cortisol concentration dependence of the normalized peak wavelength shift P_{NSK} (blue circles, left axis) and the ELISA test value R_{ELISA} (red triangles, right axis).

a)

	Collimator	Distance (mm)	SD
a)	O	30	0.0068
b)	X	15	0.0835
c)	X	30	0.0952

b)

Film height (μm)	Flow velocity (mm/s)	Equilibrium binding time (s)
2000	0	23000
500	0	6000
500	2.5	1600
500	10	1000

Table 1 a) Summary of the relationship among the collimator, the distance and the SD. b) Summary of the relationship among the film height, the flow velocity and the equilibrium binding time.